ACS APPLIED MATERIALS & INTERFACES

www.acsami.org

Research Article

# Synthesis and Electronic Applications of Particle-Templated $Ti_3C_2T_z$ MXene–Polymer Films via Pickering Emulsion Polymerization

Huaixuan Cao, Maria Escamilla, Muhammad Anas, Zeyi Tan, Siddhant Gulati, Junyeong Yun, Kailash Dhondiram Arole, Jodie L. Lutkenhaus, Miladin Radovic, Emily B. Pentzer,* and Micah J. Green*

Cite This: https://doi.org/10.1021/acsami.1c16234

Read Online

ACCESS | Metrics & More | Article Recommendations | Supporting Information



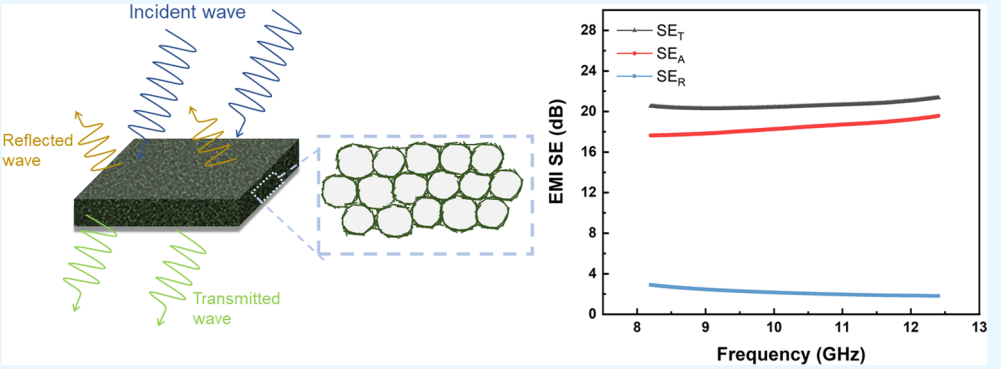


**ABSTRACT:** MXene/polymer composites have gained widespread attention due to their high electrical conductivity and extensive applications, including electromagnetic interference (EMI) shielding, energy storage, and catalysis. However, due to the difficulty of dispersing MXenes in common polymers, the fabrication of MXene/polymer composites with high electrical conductivity and satisfactory EMI shielding properties is challenging, especially at low MXene loadings. Here, we report the fabrication of MXene-armored polymer particles using dispersion polymerization in Pickering emulsions and demonstrate that these composite powders can be used as feedstocks for MXene/polymer composite films with excellent EMI shielding performance. $Ti_3C_2T_z$ nanosheets are used as the representative MXene, and three different monomers are used to prepare the armored particles. The presence of nanosheets on the particle surface was confirmed by X-ray photoelectron spectroscopy and scanning electron microscopy. Hot pressing the armored particles above $T_g$ of the polymer produced $Ti_3C_2T_z$/polymer composite films; the films are electrically conductive because of the network of nanosheets templated by the particle feedstocks. For example, the particle-templated $Ti_3C_2T_z$/polystyrene film had an electrical conductivity of 0.011 S/cm with 1.2 wt % of $Ti_3C_2T_z$, which resulted in a high radio frequency heating rate of 13−15 °C/s in the range of 135−150 MHz and an EMI shielding effectiveness of ∼21 dB within the X band. This work provides a new approach to fabricate MXene/polymer composite films with a templated electrical network at low MXene loadings.

**KEYWORDS:** *$Ti_3C_2T_z$ MXenes, Pickering emulsion, dispersion polymerization, RF heating, EMI shielding*

## INTRODUCTION

Armored particles have a polymer core coated with inorganic nanoparticles; such armored particles can be used as feedstocks for composite structures. These particles can be prepared by dispersion polymerization of the discontinuous phase of Pickering emulsions[1−7] or by the deposition of inorganic particles onto preformed polymer particles.[8−12] Two-dimensional (2D) nanosheets, including graphene oxide (GO) nanosheets and clay platelets, have been widely used to prepare armored particles, most commonly by the dispersion polymerization method. For example, the Pentzer group demonstrated the preparation of armored particles using oil-in-water emulsions stabilized by GO and UV-initiated thiol-ene polyaddition polymerization of the oil phase.[13−15] The same group used oil-in-oil emulsions stabilized by alkylated GO and thermally initiated free-radical polymerization of a methacrylate monomer as the discontinuous phase to prepare armored particles.[16,17] In a similar vein, Zhang et al. used clay platelets modified with poly [2-(dimethylamino) ethyl methacrylate] to

Received: August 27, 2021
Accepted: October 11, 2021

**Scheme 1. Overview of the Approach To Prepare $Ti_3C_2T_z$-Armored Polymer Particles and Use Them To Fabricate MXene–Polymer Composite Films with High Electrical Conductivity, Rapid RF Heating, and Good EMI Shielding Properties**

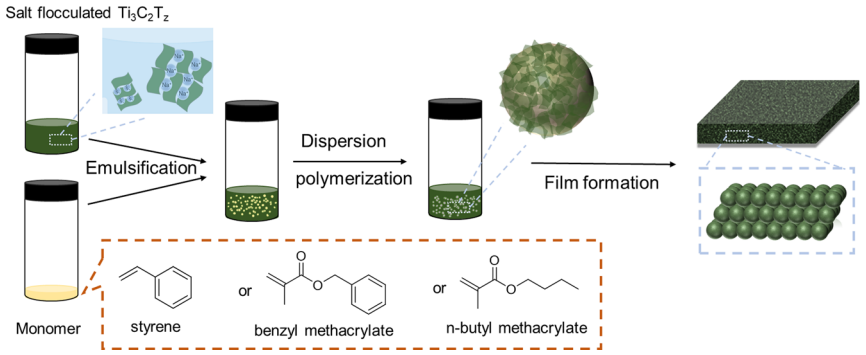


stabilize oil-in-water emulsions and dispersion polymerization to prepare polymethyl methacrylate (PMMA) particles armored with the modified clay platelets.[18] Alternatively, de Leon et al. deposited GO onto the surface of commercially available polyamide particles by "salting out" the nanosheets from an aqueous solution,[19] whereas Wu et al. used electrostatic interactions and layer-by-layer deposition of polyelectrolyte and functionalized graphene sheets to create armored hollow carbon/sulfur spheres.[11]

The use of armored particles as feedstocks for the production of composite films is most commonly achieved by hot pressing above $T_g$ of the polymer core or selective laser sintering (an additive manufacturing technique). As with most composites, the resulting films have electrical, mechanical, thermal, and barrier properties that the polymer alone does not possess.[20,21] Benefits of hot pressing are that it does not require prolonged application of high temperatures (as with melt processing), nor does it require volatile organic solvents (as with solution casting). Furthermore, hot pressing of armored particles to form films can produce an ordered structure of the inorganic particles within the film; the polymer chains of neighboring particles entangle with each other, leading to a monolithic structure, which retains the initial organization of the inorganic particles in a honeycomb-like structure at the boundaries between the polymer particles. For example, Negrete-Herrera et al. prepared polymer films using copolymer particles (styrene and n-butyl acrylate) armored with Laponite clay; by evaporating the aqueous continuous phase above $T_g$ of the copolymer, the resulting film (10 wt % clay calculated) had a honeycomb structure of nanosheets, as observed by transmission electron microscopy (TEM), and exhibited enhanced mechanical and thermal properties compared to films of the copolymer alone.[22] Similarly, Gudarzi and Sharif fabricated a GO/PMMA film by hot pressing a mixture of PMMA- and GO/PMMA-armored particles at 200 °C; the resulting film (0.3 wt % GO calculated) showed an improved thermal stability and stiffness compared to the neat polymer.[23] Alternatively, Fadil et al. used GO-armored particles with a copolymer core (styrene and n-butyl acrylate) for the preparation of an electrically conductive rGO/polymer film (5 wt % rGO calculated, 0.001 S/cm). The film was obtained by drying the dropcaste particles and then heating to 160 °C for 24 h, which had the added benefit of reducing GO nanosheets and enhancing their electrical conductivity.[24] Similarly, Merritt et al. demonstrated the use of GO-armored polystyrene particles and hot pressing at 190 °C to prepare films (2 wt % GO calculated) with excellent barrier performance to different gases at high pressure.[25]

A relatively new class of 2D nanoparticles that have been used in polymer composites but underutilized in the formation of armored particles for film formation is transition metal carbides or nitrides, referred to as MXenes. The general chemical formula of MXenes is $M_{n+1}X_nT_z$ ($n = 1–3$), where M represents an early transition metal, such as Ti or V; X is C or N; and $T_z$ represents the different functional groups on the surface (-O, -F, and -OH).[26−28] The high electrical conductivity, high catalytic activity, and rich surface functionality of MXenes enable emerging applications in energy storage, catalysis, sensing, and electromagnetic interference (EMI) shielding.[29−40] MXene/polymer composites have been prepared by both solution mixing and melt processing, with many studies addressing the electrical conductivity (Table S1)[41−50] or EMI shielding properties (Table S2)[43,44,46,50−55] of the resulting film. For example, Naguib et al. fabricated a conductive MXene/polyacrylamide (PAM) composite film by combining MXene and PAM in water and then drying the mixture under ambient conditions for 4–5 days followed by oven drying at 60 °C under vacuum (6 wt % $Ti_3C_2T_z$, 3.3 × $10^{-4}$ S/cm).[42] Liu et al. prepared a chitosan/MXene composite film by vacuum-assisted filtration of a mixture of MXene aqueous dispersion and chitosan solution followed by drying in an atmospheric environment overnight for EMI shielding (75 wt % $Ti_3C_2T_z$, 14 S/cm, 34.7 dB).[56] Similarly, Wang et al. reported a conductive MXene/epoxy composite for EMI shielding by mixing MXene with epoxy in acetone and then drying at 60 °C under vacuum and curing for 5 h at 120 °C (15 wt % $Ti_3C_2T_z$, 38 S/m, 30 dB).[52] To our knowledge, few examples focus on using MXene-armored polymer particles to prepare composite films. Qian et al. demonstrated the fabrication of a cellulose microsphere (CM)/MXene composite film for EMI shielding (66.7 wt % $Ti_3C_2T_z$, 496 S/cm, 47.1 dB) by solution mixing of CM solution with MXene aqueous dispersion and then filtering by a pressured-extrusion process followed by drying at 60 °C under vacuum for 5 min and then mechanical pressing (10 MPa) for 1 min and annealing at 400 °C for 2 h.[57] Similarly, Qian et al. prepared a cellulose nanofibril (CNF)/multiwalled carbon nanotube (MWCNT)/MXene composite film with high performance for EMI shielding (50 wt % $Ti_3C_2T_z$, 138 S/cm, 45.1 dB) by mixing CNF/MWCNT microsphere solution (prepared by spray pelletization) with MXene aqueous dispersion and filtering using a pressured-extrusion process followed by drying under vacuum for 5 min at 60 °C and annealing for 2 h at 380 °C.[58]


https://doi.org/10.1021/acsami.1c16234
ACS Appl. Mater. Interfaces XXXX, XXX, XXX−XXX

However, these two examples show the fabrication of MXene/polymer composites using a solution mixing method, which limited their use to aqueous polymer solutions. Another example was reported by Sun et al.; here, the authors prepared MXene-armored particles by leveraging electrostatic interactions between negatively charged MXenes and positively charged polystyrene-based particles and then formed films from the composite particles via compression molding (1.9 vol % $Ti_3C_2T_z$, 10.81 S/cm, 62 dB).[43] Despite these intriguing results, this approach is limited to charged polymers, and thus, the stability and properties of the resulting composite are limited. We hypothesize that dispersion polymerization of hydrophobic monomer droplets in Pickering emulsions stabilized by MXene nanosheets can provide a robust, scalable, and module approach to preparing MXene-armored particles for use as feedstocks for fabrication of composite films.

Here, we report the synthesis of $Ti_3C_2T_z$-armored polymer particles by dispersion polymerization in Pickering emulsions and their use to form composite films with high electrical conductivity, rapid radio frequency (RF) heating, and good EMI shielding properties. To develop this system, we leveraged our recent report that $Ti_3C_2T_z$-stabilized emulsions can be readily prepared when the nanosheets are flocculated with simple inorganic salts (e.g., NaCl).[59] As shown in Scheme 1, flocculated $Ti_3C_2T_z$ nanosheets were used to stabilize monomer-in-water emulsions, which underwent dispersion polymerization to give $Ti_3C_2T_z$-armored particles. The applicability of this approach to different hydrophobic monomers was demonstrated, including styrene, benzyl methacrylate, and n-butyl methacrylate. The presence of $Ti_3C_2T_z$ nanosheets on the surface of the armored particles was verified by scanning electron microscopy (SEM), X-ray photoelectron spectroscopy (XPS), and thermogravimetric analysis (TGA). Hot pressing the armored particles above $T_g$ of the core polymer processed the powder into conductive composite films. The $Ti_3C_2T_z$/PS film exhibited a high electrical conductivity of 0.011 S/cm with only 1.2 wt % of $Ti_3C_2T_z$. In contrast, solution mixing the same composition of $Ti_3C_2T_z$ and PS yielded a composite with a significantly lower conductivity ($6.3 \times 10^{-8}$ S/cm), indicating the favorable conductive network imparted by the armored particles. This conductive network, coupled with the internal structure of the $Ti_3C_2T_z$/PS film, resulted in a high RF heating rate of 13−15 °C/s within the RF range of 135−150 MHz and high EMI shielding performance (total shielding effectiveness of ∼21 dB for the X band). This work provides a new approach for producing feedstocks for MXene/polymer composites with low MXene loading and high performance, including for EMI shielding. This approach here has a distinct advantage in that any hydrophobic monomer could be used. This approach could also be extended to other MXenes (such as V-based or Nb-based nanosheets).

## MATERIALS AND METHODS

**Materials.** The $Ti_3AlC_2$ MAX phase was prepared as previously reported.[60] Lithium fluoride (LiF, 98%+) was purchased from Alfa Aesar. Hydrochloric acid (HCl, 37% [w/w], ACS reagent), dimethyl sulfoxide (DMSO, >99.5%), styrene, benzyl methacrylate (BMA), n-butyl methacrylate (n-BMA), aluminum oxide ($Al_2O_3$), and azobisisobutyronitrile (AIBN) were purchased from Sigma-Aldrich. All the monomers were purified by running through a basic alumina column to remove the inhibitors before use. AIBN was purified by recrystallization in ethanol before use.

**Instrumentation.** Emulsions were made using a hand-held emulsifier from BioSpec Products Inc. (model 985370). Optical microscopy images were obtained using an Amscope microscope. The samples were prepared by placing a drop of emulsion solution onto a glass slide. X-ray diffraction (XRD) was conducted using a Miniflex II (Rigaku) with a Cu-K$\alpha$ radiation source ($\lambda$ = 1.5406 Å), and XPS was performed using an Omicron X-ray photoelectron spectrometer employing an Mg-sourced X-ray beam at 15 kV with aperture 3. Dynamic light scattering (DLS) was performed with a Zetasizer Nano ZS90 from Malvern Instruments. TEM was conducted using an FEI Tecnai F20 transmission electron microscope operating at 200 kV. Atomic force microscopy (AFM) was conducted using a Bruker Dimension Icon AFM. SEM was performed with an FEI Quanta 600 field-emission scanning electron microscope with the acceleration voltages of 5 and 20 kV for microscopy imaging and energy-dispersive X-ray spectroscopy (EDS) imaging, respectively. TGA was conducted using a TA instrument Q50 under nitrogen flow. Differential scanning calorimetry (DSC) was performed with a TA instrument DSC 2500. The DC conductivity was obtained using a standard Keithley 4-point probe meter; RF heating was obtained using a signal generator (Rigol Inc., DSG815), a 500 W amplifier (Prana R&D, GN500D), and a fringing-field applicator (HFSS, ANSYS Inc.). The thermal image was obtained using an FLIR infrared camera (FLIR Systems Inc., A655sc). EMI shielding measurements were performed with a P5004a Keysight Streamline USB Vector Network Analyzer, 20 GHz. The sample film (2.9 cm × 1.8 cm) was fixed in-between two waveguide-to-coaxial adaptors connected face to face to measure the S-parameters ($S_{11}$ and $S_{21}$) for the calculation of shielding effectiveness (SE) and power coefficients of reflection ($R$), absorption ($A$), and transmittance ($T$).

$$SE_R = -10\log_{10}(1 - |S_{11}|^2)$$

$$SE_R = -10\log_{10}\left(\frac{|S_{21}|^2}{1 - |S_{11}|^2}\right)$$

$$SE_T = SE_R + SE_A$$

$$R = |S_{11}|^2$$

$$T = |S_{21}|^2$$

$$R + T + A = 1$$

**Preparation of $Ti_3C_2T_z$ Nanosheets.** $Ti_3C_2T_z$ nanosheets were obtained following our previously reported method.[61] Briefly, 20 mL of 6 M aqueous HCl was prepared, and 1.6 g of LiF was added with continuous stirring. Then, 2 g of MAX powder was slowly added to this solution, and the mixture was stirred continuously at 40 °C for 40 h. The resulting suspension was washed with deionized water and separated by centrifugation with the supernatant discarded. The washing process of the pellet was repeated several times until the supernatant reached pH ∼6, as determined with litmus paper. The precipitate ($Ti_3C_2T_z$ clay) was then intercalated with DMSO at room temperature for 20 h with continuous stirring. Then, excess DMSO was removed by centrifugation followed by deionized water washing 3 times and centrifugation at 9000 rpm for 26 min, discarding of the supernatant, then addition of fresh water, and bath sonication for 1 h. The $Ti_3C_2T_z$ nanosheets were obtained by centrifuging the suspension at 3500 rpm for 45 min and collecting the supernatant.

**Preparation of $Ti_3C_2T_z$ Emulsions and Armored Particles.** $Ti_3C_2T_z$-stabilized emulsions were prepared as we previously reported.[59] First, an aqueous dispersion of 1 mg/mL of $Ti_3C_2T_z$ and 0.025 M NaCl was prepared; the oil phase was prepared by dissolving 3 wt % of AIBN in the monomer (styrene, BMA, or n-BMA). For example, 27.2 mg of AIBN was dissolved in 1 mL of styrene. To prepare the emulsion, the aqueous phase and oil phase were mixed (1:5 vol/vol oil/water) and emulsified using a hand-held emulsifier (20s on, 5 s off for 3 cycles) followed by bath sonication for 1 min and then by a second emulsification using a hand-held emulsifier (20s on, 2 s off for 3 cycles). To prepare armored polymer particles, the emulsion mixture was heated to 70 °C without stirring


https://doi.org/10.1021/acsami.1c16234
ACS Appl. Mater. Interfaces XXXX, XXX, XXX−XXX

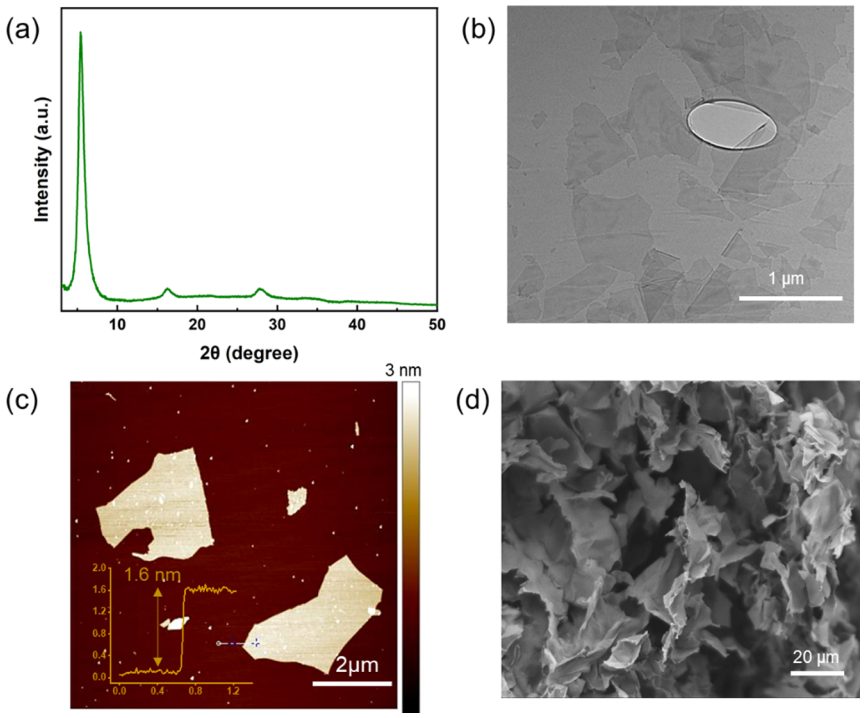


**Figure 1.** $Ti_3C_2T_z$ nanosheets: (a) XRD of the vacuum-assisted filtered film, (b) TEM of dropcast dispersion, and (c) AFM of dropcast dispersion (inset shows the thickness of the $Ti_3C_2T_z$ nanosheet along the line), and (d) SEM of freeze-dried samples.

for 24 h. The armored particles were isolated by gravity filtration, washed with deionized water and then methanol, and dried at room temperature under reduced pressure.

**Preparation of $Ti_3C_2T_z$/Polymer Films.** To prepare a 0.45 mm thick $Ti_3C_2T_z$/polymer composite film, the dried armored particles were placed in a 1.5 cm × 1.5 cm × 0.45 mm Kapton mold and then hot pressed for 5 min under high pressure (20,000 pounds) at a temperature that was ∼10 °C above polymer $T_g$. For example, we used 110 °C to hot press the $Ti_3C_2T_z$/polystyrene-armored particles to make the film. To prepare $Ti_3C_2T_z$/polymer composite films of different thicknesses, 1.25, 1.57, 2.61, and 5.19 mm thick, Teflon molds were used. For example, the $Ti_3C_2T_z$/PS particles were compressed at 110 °C under 20,000 pounds, then removed from the hot press, and cooled down to room temperature before the film was removed from the mold.

## RESULTS AND DISCUSSION

**Preparation and Characterization of $Ti_3C_2T_z$ MXenes.** $Ti_3C_2T_z$ nanosheets were chosen for this work because they are the most commonly used and widely available MXene composition. The nanosheets were prepared and characterized, as previously reported.[62] First, $Ti_3C_2T_z$ clay was prepared by selectively etching the Al layer from the parent $Ti_3AlC_2$ MAX powder using an aqueous LiF/HCl solution. $Ti_3C_2T_z$ nanosheets were then obtained by intercalation of the clay with DMSO and subsequent bath sonication, yielding a transparent, dark-green aqueous dispersion. Figure 1a shows the XRD curve of a free-standing $Ti_3C_2T_z$ nanosheet film made by vacuum-assisted filtration of the as-prepared $Ti_3C_2T_z$ dispersion. At 6 degrees, the characteristic 002 peak of $Ti_3C_2T_z$ is observed, indicating the successful etching and exfoliation of the nanosheets. Drop casting of the nanosheets and characterization by TEM show few-layer $Ti_3C_2T_z$ nanosheets, with a lateral size ranging from hundreds of nanometers to a few micrometers (Figure 1b). The average hydrodynamic diameter of $Ti_3C_2T_z$ nanosheets is ∼360 nm, indicated by DLS (Figure S1). Figure 1c shows the AFM image of $Ti_3C_2T_z$ nanosheets, with a thickness of ∼1.6 nm, indicating single-layer nanosheets. Furthermore, SEM images of a freeze-dried $Ti_3C_2T_z$ dispersion also show individual nanosheets (Figure 1d), indicating successful exfoliation.

**$Ti_3C_2T_z$-Stabilized Emulsions and $Ti_3C_2T_z$-Armored Particles.** To prepare $Ti_3C_2T_z$-armored particles, hydrophobic monomers were used to prepare oil-in-water emulsions stabilized by salt-flocculated $Ti_3C_2T_z$ followed by thermally induced dispersion polymerization. An aqueous suspension of NaCl-flocculated $Ti_3C_2T_z$ was agitated with an oil phase composed of styrene and the thermal radical initiator AIBN. Shear mixing led to the formation of a milky solution of styrene droplets in a continuous phase of water with the nanosheets located at the oil−water interface. A digital image of the emulsion (Figure 2a, inset) shows dark droplets floating atop a clear liquid, similar to our previous report and supporting associate of the nanosheets with the fluid−fluid interface. The optical microscopy image in Figure 2a reveals that the emulsion was composed of spherical droplets with a well-defined shape and of fairly uniform size.

The styrene-in-water emulsion stabilized by salt-flocculated $Ti_3C_2T_z$ was heated to 70 °C to initiate free-radical polymerization; after 24 h, the sample was cooled to room temperature, and the armored particles were characterized. The optical microscopy image in Figure 2b shows individual spherical particles with diameters similar to those of the parent emulsion droplets. As shown in Figure S2a,b, the size distributions of emulsion droplets (before polymerization) and armored particles (after polymerization) are similar, with most (>90%) of the droplet's diameter between 30 and 80 $\mu$m. Based on the emulsion composition, we expect these particles to have a solid polystyrene (PS) core and to be coated with $Ti_3C_2T_z$ ($Ti_3C_2T_z$/PS). A digital image of the vial shows the dark-green armored particles at the bottom of the vial (Figure


https://doi.org/10.1021/acsami.1c16234
ACS Appl. Mater. Interfaces XXXX, XXX, XXX−XXX

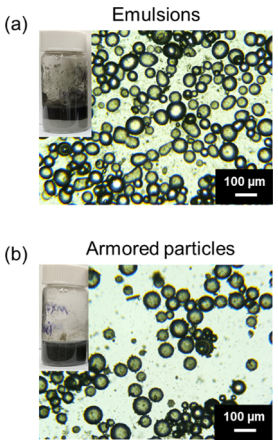


**Figure 2.** Optical microscopy images and digital images of vials (inset) of $Ti_3C_2T_z$/styrene (a) emulsions and (b) armored particles. Scale bars are 100 $\mu$m.

2b), indicating successful polymerization (the densities of styrene and PS are 0.91 and 1.05 g/mL, respectively). The $Ti_3C_2T_z$/PS-armored particles were further characterized by SEM after isolation by gravity filtration, washing, and drying under reduced pressure. The SEM images are consistent with optical microscopy images and show that the armored particles have a spherical morphology, with a diameter of 40−70 $\mu$m (Figure 3a). The SEM image in Figure 3b highlights the flaky, rough appearance of the surface of the particles, supporting the presence of $Ti_3C_2T_z$ nanosheets on the surface; in contrast, dispersion polymerization of similar emulsions stabilized by the surfactant sodium dodecyl sulfate exhibits smooth surfaces (Figure S3).

If the $Ti_3C_2T_z$/polymer particles do have a core−shell structure, $Ti_3C_2T_z$ nanosheets will be rich on the surface of the particles. EDS and XPS were used to characterize the chemical composition of the $Ti_3C_2T_z$/PS particle surface. The EDS mapping (Figure S4) of the surface of $Ti_3C_2T_z$/PS-armored particles indicates the presence of $Ti_3C_2T_z$ nanosheets, where C and Ti are uniformly distributed on the polymer sphere. The survey spectrum showed the presence of C, Ti, O, and F (Figure 3c). Deconvolution of the high-resolution Ti 2p peak into Ti−C, $Ti^{2+}$, $Ti^{3+}$, $TiO_2$, and Ti−F revealed that the $TiO_2$ peak at 458.7 eV only contributed to ∼3.7% of the Ti 2p signal (purple curve in Figure 3d). This indicates that no substantial oxidation of the $Ti_3C_2T_z$ nanosheets occurred during emulsion formation, dispersion polymerization, or isolation of the armored particles. Deconvolution of the high-resolution C 1s and O 1s peaks (Figure S5a,b) further highlights the presence of Ti−C, Ti−O, and Ti−OH bonds, which indicates that the $Ti_3C_2T_z$ nanosheet structure is retained during processing. The lack of oxidation of MXenes is critical to retention of their unique properties, including electrical conductivity; numerous methodologies for the prevention of oxidation have been developed in recent years, and the prospect of composite processing that avoids oxidation is quite promising.[62,63]

The thermal properties of $Ti_3C_2T_z$/PS-armored particles were characterized using TGA and DSC. Figure S6a shows the weight loss profile and its first derivative of $Ti_3C_2T_z$/PS particles. From 115 to 200 °C, a weight loss of ∼2.4% is observed, which may be attributed to loss of adsorbed water. The most significant weight loss is then observed from 300 to 400 °C, which is likely the decomposition of PS. For comparison, the PS particles prepared using sodium dodecyl sulfate lose a majority of mass from 280−400 °C (Figure S6b).

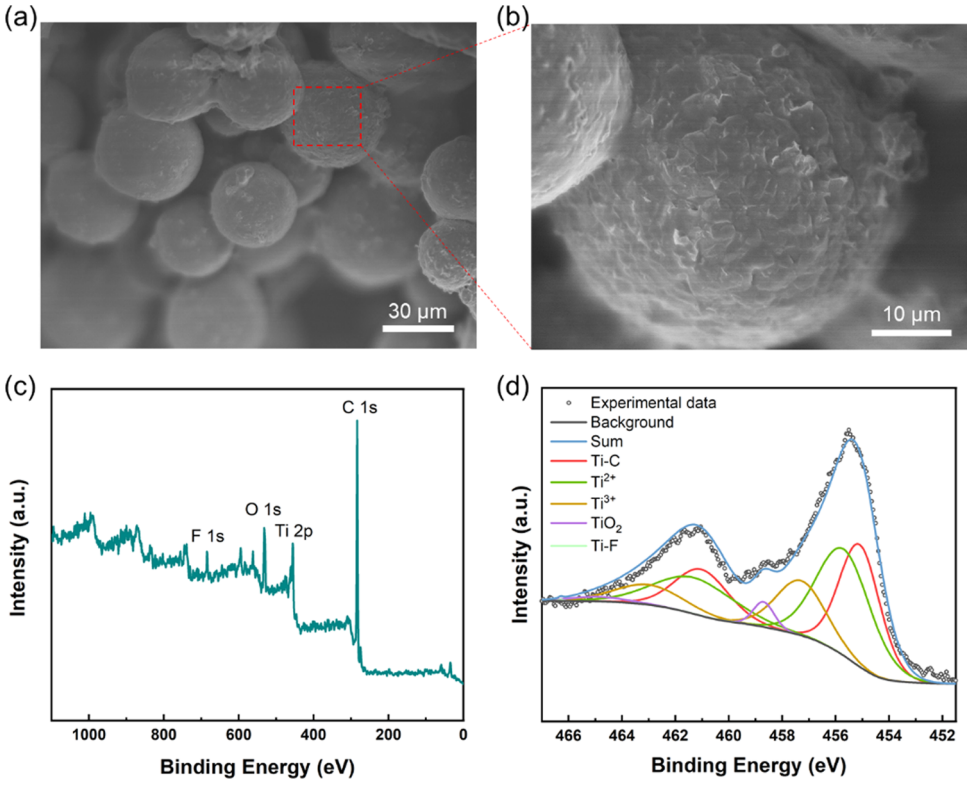


**Figure 3.** Characterization of $Ti_3C_2T_z$/PS-armored particles: (a, b) SEM images, (c) XPS survey spectrum, and (d) XPS high-resolution Ti 2p spectrum.


https://doi.org/10.1021/acsami.1c16234
ACS Appl. Mater. Interfaces XXXX, XXX, XXX−XXX

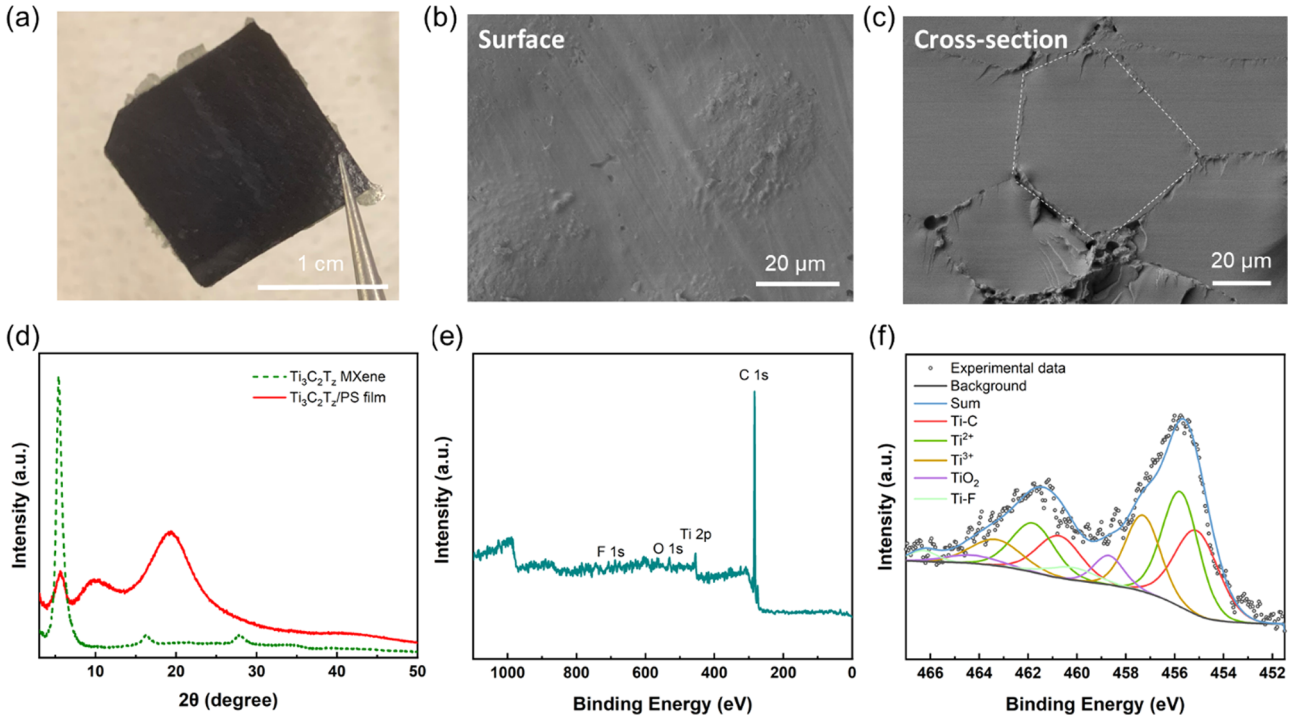


**Figure 4.** Characterization of the $Ti_3C_2T_z$/polystyrene composite film: (a) digital image, (b) SEM image of the film surface, (c) SEM image of the film cross-section, (d) XRD curves, (e) XPS survey spectrum, and (f) XPS high-resolution Ti 2p spectrum.

For the $Ti_3C_2T_z$/PS particles, a residual mass of 1.2 wt % remains after heating to 700 °C, which can be attributed to the $Ti_3C_2T_z$ nanosheets. This is in contrast to the expected weight of $Ti_3C_2T_z$ (0.55 wt %) based on the initial composition of the emulsion; this difference may be due to excess styrene in the system (incomplete encapsulation or monomer conversion), which would be removed during washing and isolation. The DSC thermogram of $Ti_3C_2T_z$/PS-armored particles in Figure S7 reveals no melting or crystallization peaks but a $T_g$ at 96 °C, in agreement with the literature value for neat PS.[64] These results indicate the presence of both $Ti_3C_2T_z$ nanosheets and PS and that $Ti_3C_2T_z$ nanosheets and the armored structure have little influence on $T_g$ of the PS.

**Film Formation and Characterization.** The $Ti_3C_2T_z$/PS-armored particles prepared by dispersion polymerization were used to prepare composite films by hot pressing the powder particles at 110 °C (i.e., above $T_g$ of PS). A digital image of the film shows a dark and uniform surface (Figure 4a). Further characterization of the morphology of the film surface by SEM revealed circular surface features with a similar size to the original PS particles (Figure 4b and Figure S8a). The cross-section images in Figure 4c and Figure S8b also show such features, suggesting that the initial organization of the $Ti_3C_2T_z$ nanosheets between the polymer spheres remains after neighboring particles fuse upon hot pressing.

The chemical composition of the $Ti_3C_2T_z$/PS film was studied by XRD and XPS. The XRD curve in Figure 4d shows the characteristic $Ti_3C_2T_z$ 002 peak around 6 degrees in the composite film (red solid line), which is consistent with pure $Ti_3C_2T_z$ (green dashed line) and indicates the presence of $Ti_3C_2T_z$ nanosheets. The XRD curve of the film also contains two broad peaks at 10 and 20 degrees, which are attributed to amorphous PS. A survey XPS spectrum of the $Ti_3C_2T_z$/PS film surface shows the presence of C, O, Ti, and F (Figure 4e); the surface sensitive nature of this technique supports that $Ti_3C_2T_z$ nanosheets are not distributed throughout the PS during film formation but instead remain localized near the surface and organized as templated by the polymer particles. Deconvolution of the high-resolution Ti 2p peak shows distinct Ti−C, $Ti^{2+}$, $Ti^{3+}$, $TiO_2$, and Ti−F (Figure 4f); as with the armored particles, the small contribution of the $TiO_2$ peak indicates that no significant oxidation occurs upon hot pressing, and supports that the conductive nature of $Ti_3C_2T_z$ is maintained during processing.

**Film Properties.** SEM, XRD, and XPS of the hot-pressed films of $Ti_3C_2T_z$/PS-armored particles indicate that the nanosheets should be electrically conductive (i.e., the nanosheets are not oxidized into insulating $TiO_2$) and that the nanosheets maintain a network between regions of solid PS. This feature is expected to result in a high electrical conductivity at low $Ti_3C_2T_z$ loadings. Using the four-point probe method, the electrical conductivity of the $Ti_3C_2T_z$/PS film was measured to be 0.011 ± 0.007 S/cm with 1.2 wt % of $Ti_3C_2T_z$. For comparison, we attempted to prepare the same film composition by drying an aqueous dispersion of $Ti_3C_2T_z$ nanosheets and PS particles and then hot pressing; this control $Ti_3C_2T_z$/PS film was nonuniform, and the separation of dark $Ti_3C_2T_z$ aggregates and the transparent polymer was obvious (Figure S9). This poor dispersion is particularly clear in the film's conductivity ($6.3 \times 10^{-8}$ S/cm) that was significantly lower than that of the $Ti_3C_2T_z$/PS film made by hot pressing the armored particles (0.011 S/cm). We attribute the increased performance of the armored particle film to the templated formation of a network of nanosheets during hot pressing, similar to what has been reported for reduced rGO-armored particles.[24] To our knowledge, the electrical conductivity of our armored particle-derived $Ti_3C_2T_z$/PS film is comparable to the literature values of the MXene/polymer composite film with a similar MXene loading (Table S3).[42,43,45,49,50] However, most of the reported films are prepared using the solvent


https://doi.org/10.1021/acsami.1c16234
ACS Appl. Mater. Interfaces XXXX, XXX, XXX−XXX

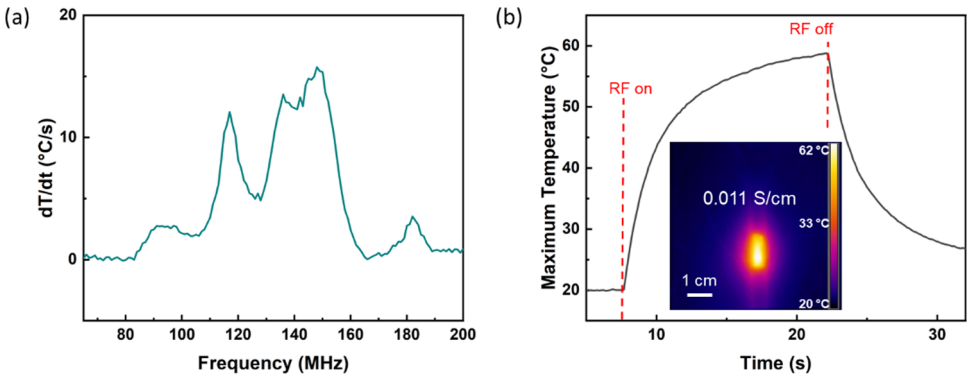


**Figure 5.** RF heating of the $Ti_3C_2T_z$/PS composite film: (a) frequency sweep, (b) RF heating curve at 135 MHz, 0.1 W; the inset shows the thermal image of the film.

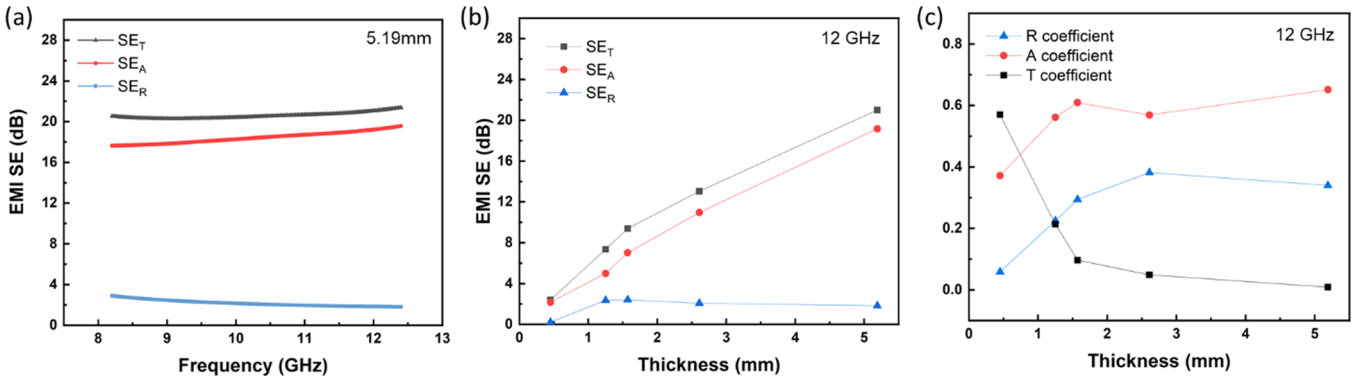


**Figure 6.** EMI shielding effectiveness of the $Ti_3C_2T_z$/PS composite film (a) with a thickness of 5.19 mm and (b) as a function of film thickness at 12 GHz. (c) EMI shielding power coefficients of reflection ($R$), absorption ($A$), and transmittance ($T$).

mixing method, which requires organic solvents (e.g., DMF and DMSO) when nonwater dispersible polymers are desired. Thus, using emulsions to architect armored particles can readily produce feedstocks for $Ti_3C_2T_z$/PS composite films with high conductivity and low $Ti_3C_2T_z$ loading using water and without organic solvents.

In addition to the DC conductivity measurement, RF heating was demonstrated for the $Ti_3C_2T_z$/PS film. Figure 5a shows heating rates as a function of RF at 0.1 W. The maximum heating rate of around 15 °C/s is observed at a frequency of 150 MHz, which corresponds to the maximum absorption of RF fields. Other heating peaks at 117 MHz and in the range of 135−150 MHz are observed. This shows that heating can be modulated with frequency. Figure 5b shows one RF heating cycle of the $Ti_3C_2T_z$/PS film at 135 MHz at 0.1 W. Interestingly, while the pure PS film (nonconductive) and the control $Ti_3C_2T_z$/PS film ($6.3 \times 10^{-8}$ S/cm) do not heat under these conditions, the $Ti_3C_2T_z$/PS film heats rapidly in response to a low power RF field: from 25 to 60 °C in a few seconds at only 0.1 W. These data indicate the formation of an electrically conductive network in the $Ti_3C_2T_z$/PS film, which is further revealed by the uniform heating throughout the film, as shown in the inset thermal image; this is consistent with our prior work on $Ti_3C_2T_z$/polymer composites[65] where $Ti_3C_2T_z$ was solution mixed with poly(vinyl alcohol), and vacuum-assisted filtration was used to prepare a composite film of 25 wt % $Ti_3C_2T_z$, but in the current study, the composite contains only 1.2 wt % $Ti_3C_2T_z$. Thus, compared to solution-mixed $Ti_3C_2T_z$/polymer composite films, our particle-templated film showed a significantly enhanced RF heating response at low $Ti_3C_2T_z$ loading.

Additionally, the EMI shielding performance of the $Ti_3C_2T_z$/PS composite film was investigated in the 8.2 to 12.4 GHz range. As shown in Figure 6a, the SE of a 5.19 mm $Ti_3C_2T_z$/PS film (1.2 wt % of $Ti_3C_2T_z$) was ∼21 dB for the X band, which satisfies the minimum requirement for commercial use.[46] For comparison, the control $Ti_3C_2T_z$/PS film cannot be measured for EMI shielding due to low conductivity ($6.3 \times 10^{-8}$ S/cm). Also, Figure 6a shows that the SE adsorption and SE reflection values are ∼18 and ∼3 dB, respectively, indicating that the EMI shielding of the $Ti_3C_2T_z$/PS film might conform to an adsorption-dominated mechanism. The relationship between SE and sample thickness is shown in Figure 6b. Generally, SE increases with thickness due to the increased adsorption of electromagnetic waves. Here, for $Ti_3C_2T_z$/PS films with thicknesses of 1.57, 2.61, and 5.19 mm, total SE values of 9.4, 13, and 21 dB are observed at 12 GHz, respectively, and the absorption SE values across the same samples are 7, 11, and 19 dB. Thus, the EMI shielding performance of our $Ti_3C_2T_z$/PS composite films is attributed to the compact and conductive network provided by the armored particle feedstocks.

We next investigate the mechanism of EMI shielding of the $Ti_3C_2T_z$/PS film. An electromagnetic wave is partially reflected and partially absorbed when hitting the shielding material, while the rest is transmitted through the material. Their corresponding power coefficients of reflection ($R$), absorption ($A$), and transmittance ($T$) indicate the ability of the shielding material to reflect, absorb, or transmit electromagnetic waves.[66]


https://doi.org/10.1021/acsami.1c16234
ACS Appl. Mater. Interfaces XXXX, XXX, XXX−XXX

$R$, $A$, and $T$ coefficients are calculated based on their S-parameters ($S_{11}$ and $S_{21}$). As shown in Figure 6c, with the increase of the film thickness, the $A$ and $R$ coefficients increase at small thickness (< ~2 mm), and no substantial change is observed when the film thickness is greater than ~2 mm, while the $T$ coefficient decreases dramatically at small thickness till ~2 mm and then slowly decreases till ~5 mm. For all thickness values, the $A$ coefficient is larger than the $R$ coefficient, indicating the $Ti_3C_2T_z$/PS film's absorption behavior relative to reflection. This result confirms the absorption-dominated EMI shielding mechanism of our $Ti_3C_2T_z$/PS film.

**Applicability to Other Polymers.** The temperature of processing armored particles into films is dictated by $T_g$ of the polymer, and thus, the ability to access $Ti_3C_2T_z$-armored particles with other polymer cores broadens the usefulness of the system. Dispersion free-radical polymerization to prepare armored particles can be used with monomers that are not miscible with water when they are used as the oil phase in $Ti_3C_2T_z$-stabilized Pickering emulsions (Scheme 1). Using the same polymerization conditions as for styrene, BMA and n-BMA were used to prepare $Ti_3C_2T_z$/PBMA- and $Ti_3C_2T_z$/PnBMA-armored particles, respectively. These armored particles were characterized by optical microscopy and SEM imaging, as well as XPS (Figures S10–S12); all samples were composed of discrete spherical armored particles, and XPS showed the presence of $Ti_3C_2T_z$ near the surface and that no significant oxidation of the nanosheets took place. We then demonstrated that the different armored particles could be used to form electrically conductive polymer composites by hot pressing, with the temperature used for each dictated by $T_g$ of the polymer; $Ti_3C_2T_z$/PBMA was processed at 65 °C ($T_g$ = 57 °C), and $Ti_3C_2T_z$/PnBMA was processed at 35 °C ($T_g$ = 27 °C). Both of the resulting composite films were electrically conductive: 0.015 and 0.006 S/cm for $Ti_3C_2T_z$/PBMA and $Ti_3C_2T_z$/PnBMA, respectively. Surface and cross-sectional SEM images of these films indicate a $Ti_3C_2T_z$ percolating network, as observed with the $Ti_3C_2T_z$/PS films (Figure S13).

## CONCLUSIONS

$Ti_3C_2T_z$/PS-armored particles were synthesized by dispersion polymerization in Pickering emulsions and used to prepare composite films with low $Ti_3C_2T_z$ loading (~1.2 wt %) and high conductivity, rapid RF heating, and good EMI shielding capabilities. NaCl-flocculated $Ti_3C_2T_z$ nanosheets were used to stabilize monomer-in-water emulsions and polymerization of the droplet monomer phase in the emulsion-formed $Ti_3C_2T_z$-armored polymer particles. The $Ti_3C_2T_z$/PS core–shell structure was verified by SEM, XPS, and TGA, and the structure of these particles did not significantly impact $T_g$ of the polymer core. Hot pressing these armored particles at 110 °C yielded electrically conductive $Ti_3C_2T_z$/polymer composite films; characterization by SEM revealed circular features on both the surface and cross-section of the film, supporting the formation of a network of $Ti_3C_2T_z$ nanosheets templated by the particles. The chemical structure of the nanosheets was verified by XRD and XPS, indicating a lack of oxidation. The electrical conductivity of the $Ti_3C_2T_z$/PS film was 0.011 S/cm, which results in a rapid RF heating rate (13–15 °C/s) in the ratio frequency range of 135–150 MHz. Furthermore, these structured composite films with a thickness of 5.19 mm showed a high EMI SE of 21 dB, with an adsorption-dominated shielding mechanism. The use of other polymers allows for the temperature of processing to be controlled, and films were formed from $Ti_3C_2T_z$-armored particles of poly(benzyl methacrylate) ($T_g$ = 57 °C) and poly(n-butyl methacrylate) ($T_g$ = 27 °C). This particle-templated approach to the preparation of the MXene/polymer film gives access to ordered MXene networks within the composite film and overcomes the propensity of nanosheets to aggregate or restack, as observed in melt processing and solution blending, thereby giving enhanced electrical properties at low MXene loading. Furthermore, this approach avoids the use of organic solvents and expands the range of accessible MXene/polymer compositions for diverse and tailored applications.

## ASSOCIATED CONTENT

### Supporting Information

The Supporting Information is available free of charge at https://pubs.acs.org/doi/10.1021/acsami.1c16234.

Table of conductivity of MXene/polymer composites using different processing methods, table of EMI shielding SE of MXene/polymer composites, DLS of aqueous nanosheet dispersions, additional optical microscopy images and size distribution of emulsions and armored particles, additional SEM and EDS mapping of armored particles, high-resolution XPS spectra of armored particles, TGA of armored particles, DSC of armored particles, table of conductivity of MXene/polymer composites at MXene loadings close to 1.2 wt %, optical microscopy images, and SEM and XPS of composite particles and films (PDF)

## AUTHOR INFORMATION


### Corresponding Authors

**Emily B. Pentzer** − *Department of Materials Science and Engineering and Department of Chemistry, Texas A&M University, College Station, Texas 77843, United States;* orcid.org/0000-0001-6187-6135; Email: emilypentzer@tamu.edu

**Micah J. Green** − *Artie McFerrin Department of Chemical Engineering and Department of Materials Science and Engineering, Texas A&M University, College Station, Texas 77843, United States;* orcid.org/0000-0001-5691-0861; Email: micah.green@tamu.edu

### Authors

**Huaixuan Cao** − *Artie McFerrin Department of Chemical Engineering, Texas A&M University, College Station, Texas 77843, United States*

**Maria Escamilla** − *Department of Materials Science and Engineering, Texas A&M University, College Station, Texas 77843, United States*

**Muhammad Anas** − *Artie McFerrin Department of Chemical Engineering, Texas A&M University, College Station, Texas 77843, United States*

**Zeyi Tan** − *Department of Materials Science and Engineering, Texas A&M University, College Station, Texas 77843, United States*

**Siddhant Gulati** − *Artie McFerrin Department of Chemical Engineering, Texas A&M University, College Station, Texas 77843, United States*

**Junyeong Yun** − *Artie McFerrin Department of Chemical Engineering, Texas A&M University, College Station, Texas 77843, United States*




https://doi.org/10.1021/acsami.1c16234
ACS Appl. Mater. Interfaces XXXX, XXX, XXX−XXX

**Kailash Dhondiram Arole** − *Department of Materials Science and Engineering, Texas A&M University, College Station, Texas 77843, United States;* orcid.org/0000-0002-4516-889X

**Jodie L. Lutkenhaus** − *Artie McFerrin Department of Chemical Engineering and Department of Materials Science and Engineering, Texas A&M University, College Station, Texas 77843, United States;* orcid.org/0000-0002-2613-6016

**Miladin Radovic** − *Department of Materials Science and Engineering, Texas A&M University, College Station, Texas 77843, United States*

Complete contact information is available at: https://pubs.acs.org/10.1021/acsami.1c16234

### Author Contributions

The manuscript was written through contributions of all authors. All authors have given approval to the final version of the manuscript.

### Notes

The authors declare no competing financial interest.

## ■ ACKNOWLEDGMENTS

The authors thank Texas A&M University for financial support. E.B.P. thanks NSF DMR CAREER award #1955170. We would like to thank TAMU Materials Characterization Facilities for use of XPS, AFM, SEM, and EDS, Soft Matter Facility for use of TGA and DSC, and Microscopy and Imaging Center for use of TEM. We also thank Dr. Mustafa Akbulut's group and graduate student Shuhao Liu at Texas A&M University for the help in use of the Zetasizer instrument. We acknowledge the help from Xiaofei Zhao in the synthesis process of MXenes.

## ■ REFERENCES

(1) Bourgeat-Lami, E.; Guimarães, T. R.; Pereira, A. M. C.; Alves, G. M.; Moreira, J. C.; Putaux, J.-L.; dos Santos, A. M. High Solids Content, Soap-Free, Film-Forming Latexes Stabilized by Laponite Clay Platelets. *Macromol. Rapid Commun.* **2010**, *31*, 1874−1880.

(2) Delafresnaye, L.; Dugas, P.-Y.; Dufils, P.-E.; Chaduc, I.; Vinas, J.; Lansalot, M.; Bourgeat-Lami, E. Synthesis of clay-armored poly(vinylidene chloride-co-methyl acrylate) latexes by Pickering emulsion polymerization and their film-forming properties. *Polym. Chem.* **2017**, *8*, 6217−6232.

(3) Li, H.; Zhou, J.; Zhao, J.; Li, Y.; Lu, K. Synthesis of cellulose nanocrystals-armored fluorinated polyacrylate latexes via Pickering emulsion polymerization and their film properties. *Colloids Surf. B: Biointerfaces* **2020**, *192*, No. 111071.

(4) Li, K.; Xie, L.; Wang, B.; Yan, J.; Tang, H.; Zhou, D. Mechanistic Investigation of Surfactant-Free Emulsion Polymerization Using Magnetite Nanoparticles Modified by Citric Acid as Stabilizers. *Langmuir* **2020**, *36*, 8290−8300.

(5) Limousin, E.; Ballard, N.; Asua, J. M. Synthesis of cellulose nanocrystal armored latex particles for mechanically strong nanocomposite films. *Polym. Chem.* **2019**, *10*, 1823−1831.

(6) Qiao, X. G.; Dugas, P. Y.; Prevot, V.; Bourgeat-Lami, E. Surfactant-free synthesis of layered double hydroxide-armored latex particles. *Polym. Chem.* **2020**, *11*, 3195−3208.

(7) Teixeira, R. F. A.; McKenzie, H. S.; Boyd, A. A.; Bon, S. A. F. Pickering Emulsion Polymerization Using Laponite Clay as Stabilizer To Prepare Armored "Soft" Polymer Latexes. *Macromolecules* **2011**, *44*, 7415−7422.

(8) Correa-Duarte, M. A.; Kosiorek, A.; Kandulski, W.; Giersig, M.; Salgueiriño-Maceira, V. Nanoengineered Polymeric Thin Films by Sintering CNT-Coated Polystyrene Spheres. *Small* **2006**, *2*, 220−224.

(9) Gharieh, A.; Moghadas, M.; Pourghasem, M. Synergistic Effects of Acrylic/Silica Armored Structured Nanoparticles on the Toughness and Physicomechanical Properties of Epoxy Polymers. *ACS Appl. Polym. Mater.* **2021**, *3*, 4008−4016.

(10) Lipton, J.; Weng, G.-M.; Röhr, J. A.; Wang, H.; Taylor, A. D. Layer-by-Layer Assembly of Two-Dimensional Materials: Meticulous Control on the Nanoscale. *Matter* **2020**, *2*, 1148−1165.

(11) Wu, F.; Li, J.; Su, Y.; Wang, J.; Yang, W.; Li, N.; Chen, L.; Chen, S.; Chen, R.; Bao, L. Layer-by-Layer Assembled Architecture of Polyelectrolyte Multilayers and Graphene Sheets on Hollow Carbon Spheres/Sulfur Composite for High-Performance Lithium−Sulfur Batteries. *Nano Lett.* **2016**, *16*, 5488−5494.

(12) Zhao, M.-Q.; Xie, X.; Ren, C. E.; Makaryan, T.; Anasori, B.; Wang, G.; Gogotsi, Y. Hollow MXene Spheres and 3D Macroporous MXene Frameworks for Na-Ion Storage. *Adv. Mater.* **2017**, *29*, 1702410.

(13) Rodier, B. J.; Mosher, E. P.; Burton, S. T.; Matthews, R.; Pentzer, E. Polythioether Particles Armored with Modifiable Graphene Oxide Nanosheets. *Macromol. Rapid Commun.* **2016**, *37*, 894−899.

(14) Edgehouse, K.; Escamilla, M.; Wang, L.; Dent, R.; Pachuta, K.; Kendall, L.; Wei, P.; Sehirlioglu, A.; Pentzer, E. Stabilization of oil-in-water emulsions with graphene oxide and cobalt oxide nanosheets and preparation of armored polymer particles. *J. Colloid Interface Sci.* **2019**, *541*, 269−278.

(15) Wei, P.; Luo, Q.; Edgehouse, K. J.; Hemmingsen, C. M.; Rodier, B. J.; Pentzer, E. B. 2D Particles at Fluid−Fluid Interfaces: Assembly and Templating of Hybrid Structures for Advanced Applications. *ACS Appl. Mater. Interfaces* **2018**, *10*, 21765−21781.

(16) Rodier, B. J.; de Leon, A.; Hemmingsen, C.; Pentzer, E. Polymerizations in oil-in-oil emulsions using 2D nanoparticle surfactants. *Polym. Chem.* **2018**, *9*, 1547−1550.

(17) Zia, A.; Pentzer, E.; Thickett, S.; Kempe, K. Advances and Opportunities of Oil-in-Oil Emulsions. *ACS Appl. Mater. Interfaces* **2020**, *12*, 38845−38861.

(18) Zhang, J.; Chen, K.; Zhao, H. PMMA colloid particles armored by clay layers with PDMAEMA polymer brushes. *J. Polym. Sci. A Polym. Chem.* **2008**, *46*, 2632−2639.

(19) de Leon, A. C.; Rodier, B. J.; Bajamundi, C.; Espera, A., Jr.; Wei, P.; Kwon, J. G.; Williams, J.; Ilijasic, F.; Advincula, R. C.; Pentzer, E. Plastic Metal-Free Electric Motor by 3D Printing of Graphene-Polyamide Powder. *ACS Appl. Energy Mater.* **2018**, *1*, 1726−1733.

(20) Tarhini, A. A.; Tehrani-Bagha, A. R. Graphene-based polymer composite films with enhanced mechanical properties and ultra-high in-plane thermal conductivity. *Compos. Sci. Technol.* **2019**, *184*, 107797.

(21) Gong, K.; Zhou, K.; Qian, X.; Shi, C.; Yu, B. MXene as emerging nanofillers for high-performance polymer composites: A review. *Compos. Part B: Eng.* **2021**, *217*, No. 108867.

(22) Negrete-Herrera, N.; Putaux, J.-L.; David, L.; Haas, F. D.; Bourgeat-Lami, E. Polymer/Laponite Composite Latexes: Particle Morphology, Film Microstructure, and Properties. *Macromol. Rapid Commun.* **2007**, *28*, 1567−1573.

(23) Gudarzi, M. M.; Sharif, F. Self assembly of graphene oxide at the liquid−liquid interface: A new route to the fabrication of graphene based composites. *Soft Matter* **2011**, *7*, 3432−3440.

(24) Fadil, Y.; Agarwal, V.; Jasinski, F.; Thickett, S. C.; Minami, H.; Zetterlund, P. B. Electrically conductive polymer/rGO nanocomposite films at ambient temperature via miniemulsion polymerization using GO as surfactant. *Nanoscale* **2019**, *11*, 6566−6570.

(25) Merritt, S. M. J.; Wemyss, A. M.; Farris, S.; Patole, S.; Patias, G.; Haddleton, D. M.; Shollock, B.; Wan, C. Gas Barrier Polymer Nanocomposite Films Prepared by Graphene Oxide Encapsulated Polystyrene Microparticles. *ACS Appl. Polym. Mater.* **2020**, *2*, 725−731.

(26) Naguib, M.; Kurtoglu, M.; Presser, V.; Lu, J.; Niu, J.; Heon, M.; Hultman, L.; Gogotsi, Y.; Barsoum, M. W. Two-Dimensional

Nanocrystals Produced by Exfoliation of Ti3AlC2. *Adv. Mater.* **2011**, *23*, 4248−4253.
(27) Naguib, M.; Mochalin, V. N.; Barsoum, M. W.; Gogotsi, Y. 25th Anniversary Article: MXenes: A New Family of Two-Dimensional Materials. *Adv. Mater.* **2014**, *26*, 992−1005.
(28) Ghidiu, M.; Lukatskaya, M. R.; Zhao, M.-Q.; Gogotsi, Y.; Barsoum, M. W. Conductive two-dimensional titanium carbide 'clay' with high volumetric capacitance. *Nature* **2014**, *516*, 78−81.
(29) Anasori, B.; Lukatskaya, M. R.; Gogotsi, Y. 2D metal carbides and nitrides (MXenes) for energy storage. *Nat. Rev. Mater.* **2017**, *2*, 16098.
(30) Boota, M.; Anasori, B.; Voigt, C.; Zhao, M.-Q.; Barsoum, M. W.; Gogotsi, Y. Pseudocapacitive Electrodes Produced by Oxidant-Free Polymerization of Pyrrole between the Layers of 2D Titanium Carbide (MXene). *Adv. Mater.* **2016**, *28*, 1517−1522.
(31) Cheng, L.; Li, X.; Zhang, H.; Xiang, Q. Two-Dimensional Transition Metal MXene-Based Photocatalysts for Solar Fuel Generation. *J. Phys. Chem. Lett.* **2019**, *10*, 3488−3494.
(32) Gao, G.; O'Mullane, A. P.; Du, A. 2D MXenes: A New Family of Promising Catalysts for the Hydrogen Evolution Reaction. *ACS Catal.* **2017**, *7*, 494−500.
(33) Iqbal, A.; Kwon, J.; Kim, M. K.; Koo, C. M. MXenes for electromagnetic interference shielding: Experimental and theoretical perspectives. *Mater. Today Adv.* **2021**, *9*, 100124.
(34) Lukatskaya, M. R.; Kota, S.; Lin, Z.; Zhao, M.-Q.; Shpigel, N.; Levi, M. D.; Halim, J.; Taberna, P.-L.; Barsoum, M. W.; Simon, P.; Gogotsi, Y. Ultra-high-rate pseudocapacitive energy storage in two-dimensional transition metal carbides. *Nat. Energy* **2017**, *2*, 17105.
(35) Naguib, M.; Mashtalir, O.; Carle, J.; Presser, V.; Lu, J.; Hultman, L.; Gogotsi, Y.; Barsoum, M. W. Two-Dimensional Transition Metal Carbides. *ACS Nano* **2012**, *6*, 1322−1331.
(36) Orangi, J.; Hamade, F.; Davis, V. A.; Beidaghi, M. 3D Printing of Additive-Free 2D Ti3C2Tx (MXene) Ink for Fabrication of Micro-Supercapacitors with Ultra-High Energy Densities. *ACS Nano* **2020**, *14*, 640−650.
(37) Pei, Y.; Zhang, X.; Hui, Z.; Zhou, J.; Huang, X.; Sun, G.; Huang, W. Ti3C2TX MXene for Sensing Applications: Recent Progress, Design Principles, and Future Perspectives. *ACS Nano* **2021**, *15*, 3996−4017.
(38) Shahzad, F.; Alhabeb, M.; Hatter, C. B.; Anasori, B.; Man Hong, S.; Koo, C. M.; Gogotsi, Y. Electromagnetic interference shielding with 2D transition metal carbides (MXenes). *Science* **2016**, *353*, 1137.
(39) Song, P.; Liu, B.; Qiu, H.; Shi, X.; Cao, D.; Gu, J. MXenes for polymer matrix electromagnetic interference shielding composites: A review. *Compos. Commun.* **2021**, *24*, 100653.
(40) Zhou, Z.; Panatdasirisuk, W.; Mathis, T. S.; Anasori, B.; Lu, C.; Zhang, X.; Liao, Z.; Gogotsi, Y.; Yang, S. Layer-by-layer assembly of MXene and carbon nanotubes on electrospun polymer films for flexible energy storage. *Nanoscale* **2018**, *10*, 6005−6013.
(41) Ling, Z.; Ren, C. E.; Zhao, M.-Q.; Yang, J.; Giammarco, J. M.; Qiu, J.; Barsoum, M. W.; Gogotsi, Y. Flexible and conductive MXene films and nanocomposites with high capacitance. *Proc. Natl. Acad. Sci. U. S. A.* **2014**, *111*, 16676.
(42) Naguib, M.; Saito, T.; Lai, S.; Rager, M. S.; Aytug, T.; Parans Paranthaman, M.; Zhao, M.-Q.; Gogotsi, Y. Ti3C2Tx (MXene)−polyacrylamide nanocomposite films. *RSC Adv.* **2016**, *6*, 72069−72073.
(43) Sun, R.; Zhang, H.-B.; Liu, J.; Xie, X.; Yang, R.; Li, Y.; Hong, S.; Yu, Z.-Z. Highly Conductive Transition Metal Carbide/Carbonitride-(MXene)@polystyrene Nanocomposites Fabricated by Electrostatic Assembly for Highly Efficient Electromagnetic Interference Shielding. *Adv. Funct. Mater.* **2017**, *27*, 1702807.
(44) Cao, W.-T.; Chen, F.-F.; Zhu, Y.-J.; Zhang, Y.-G.; Jiang, Y.-Y.; Ma, M.-G.; Chen, F. Binary Strengthening and Toughening of MXene/Cellulose Nanofiber Composite Paper with Nacre-Inspired Structure and Superior Electromagnetic Interference Shielding Properties. *ACS Nano* **2018**, *12*, 4583−4593.
(45) Tu, S.; Jiang, Q.; Zhang, X.; Alshareef, H. N. Large Dielectric Constant Enhancement in MXene Percolative Polymer Composites. *ACS Nano* **2018**, *12*, 3369−3377.
(46) Luo, J.-Q.; Zhao, S.; Zhang, H.-B.; Deng, Z.; Li, L.; Yu, Z.-Z. Flexible, stretchable and electrically conductive MXene/natural rubber nanocomposite films for efficient electromagnetic interference shielding. *Compos. Sci. Technol.* **2019**, *182*, 107754.
(47) Mazhar, S.; Qarni, A. A.; Ul Haq, Y.; Ul Haq, Z.; Murtaza, I. Promising PVC/MXene based flexible thin film nanocomposites with excellent dielectric, thermal and mechanical properties. *Ceram. Int.* **2020**, *46*, 12593−12605.
(48) Seyedin, S.; Uzun, S.; Levitt, A.; Anasori, B.; Dion, G.; Gogotsi, Y.; Razal, J. M. MXene Composite and Coaxial Fibers with High Stretchability and Conductivity for Wearable Strain Sensing Textiles. *Adv. Funct. Mater.* **2020**, *30*, 1910504.
(49) Wang, D.; Lin, Y.; Hu, D.; Jiang, P.; Huang, X. Multifunctional 3D-MXene/PDMS nanocomposites for electrical, thermal and triboelectric applications. *Compos. Part A: Appl. Sci. Manuf.* **2020**, *130*, 105754.
(50) Xu, M.-K.; Liu, J.; Zhang, H.-B.; Zhang, Y.; Wu, X.; Deng, Z.; Yu, Z.-Z. Electrically Conductive Ti3C2Tx MXene/Polypropylene Nanocomposites with an Ultralow Percolation Threshold for Efficient Electromagnetic Interference Shielding. *Ind. Eng. Chem. Res.* **2021**, *60*, 4342−4350.
(51) Han, M.; Yin, X.; Wu, H.; Hou, Z.; Song, C.; Li, X.; Zhang, L.; Cheng, L. Ti3C2 MXenes with Modified Surface for High-Performance Electromagnetic Absorption and Shielding in the X-Band. *ACS Appl. Mater. Interfaces* **2016**, *8*, 21011−21019.
(52) Wang, L.; Chen, L.; Song, P.; Liang, C.; Lu, Y.; Qiu, H.; Zhang, Y.; Kong, J.; Gu, J. Fabrication on the annealed Ti3C2Tx MXene/Epoxy nanocomposites for electromagnetic interference shielding application. *Compos. Part B: Eng.* **2019**, *171*, 111−118.
(53) Xu, H.; Yin, X.; Li, X.; Li, M.; Liang, S.; Zhang, L.; Cheng, L. Lightweight Ti2CTx MXene/Poly(vinyl alcohol) Composite Foams for Electromagnetic Wave Shielding with Absorption-Dominated Feature. *ACS Appl. Mater. Interfaces* **2019**, *11*, 10198−10207.
(54) Rajavel, K.; Luo, S.; Wan, Y.; Yu, X.; Hu, Y.; Zhu, P.; Sun, R.; Wong, C. 2D Ti3C2Tx MXene/polyvinylidene fluoride (PVDF) nanocomposites for attenuation of electromagnetic radiation with excellent heat dissipation. *Compos. Part A: Appl. Sci. Manuf.* **2020**, *129*, 105693.
(55) Ma, W.; Cai, W.; Chen, W.; Liu, P.; Wang, J.; Liu, Z. A novel structural design of shielding capsule to prepare high-performance and self-healing MXene-based sponge for ultra-efficient electromagnetic interference shielding. *Chem. Eng. J.* **2021**, *426*, 130729.
(56) Liu, F.; Li, Y.; Hao, S.; Cheng, Y.; Zhan, Y.; Zhang, C.; Meng, Y.; Xie, Q.; Xia, H. Well-aligned MXene/chitosan films with humidity response for high-performance electromagnetic interference shielding. *Carbohydr. Polym.* **2020**, *243*, 116467.
(57) Qian, K.; Zhou, Q.; Wu, H.; Fang, J.; Miao, M.; Yang, Y.; Cao, S.; Shi, L.; Feng, X. Carbonized cellulose microsphere@void@MXene composite films with egg-box structure for electromagnetic interference shielding. *Compos. Part A: Appl. Sci. Manuf.* **2021**, *141*, 106229.
(58) Qian, K.; Wu, H.; Fang, J.; Yang, Y.; Miao, M.; Cao, S.; Shi, L.; Feng, X. Yarn-ball-shaped CNF/MWCNT microspheres intercalating Ti3C2Tx MXene for electromagnetic interference shielding films. *Carbohydr. Polym.* **2021**, *254*, 117325.
(59) Cao, H.; Escamilla, M.; Arole, K. D.; Holta, D.; Lutkenhaus, J. L.; Radovic, M.; Green, M. J.; Pentzer, E. B. Flocculation of MXenes and Their Use as 2D Particle Surfactants for Capsule Formation. *Langmuir* **2021**, *37*, 2649−2657.
(60) Gao, H.; Benitez, R.; Son, W.; Arroyave, R.; Radovic, M. Structural, physical and mechanical properties of Ti3(Al1−xSix)C2 solid solution with x=0−1. *Mater. Sci. Eng.: A* **2016**, *676*, 197−208.
(61) Shah, S. A.; Habib, T.; Gao, H.; Gao, P.; Sun, W.; Green, M. J.; Radovic, M. Template-free 3D titanium carbide (Ti3C2Tx) MXene particles crumpled by capillary forces. *Chem. Commun.* **2017**, *53*, 400−403.


https://doi.org/10.1021/acsami.1c16234
ACS Appl. Mater. Interfaces XXXX, XXX, XXX−XXX

(62) Zhao, X.; Vashisth, A.; Prehn, E.; Sun, W.; Shah, S. A.; Habib, T.; Chen, Y.; Tan, Z.; Lutkenhaus, J. L.; Radovic, M.; Green, M. J. Antioxidants Unlock Shelf-Stable Ti3C2Tx (MXene) Nanosheet Dispersions. *Matter* **2019**, *1*, 513−526.
(63) Habib, T.; Zhao, X.; Shah, S. A.; Chen, Y.; Sun, W.; An, H.; Lutkenhaus, J. L.; Radovic, M.; Green, M. J. Oxidation stability of Ti3C2Tx MXene nanosheets in solvents and composite films. *npj 2D Mater. Appl.* **2019**, *3*, 8.
(64) Mark, J. E., *Polymer Data Handbook* (2nd Edition); Oxford University Press: 2009, 830.
(65) Habib, T.; Patil, N.; Zhao, X.; Prehn, E.; Anas, M.; Lutkenhaus, J. L.; Radovic, M.; Green, M. J. Heating of Ti3C2Tx MXene/polymer composites in response to Radio Frequency fields. *Sci. Rep.* **2019**, *9*, 16489.
(66) Wan, Y.-J.; Zhu, P.-L.; Yu, S.-H.; Sun, R.; Wong, C.-P.; Liao, W.-H. Anticorrosive, Ultralight, and Flexible Carbon-Wrapped Metallic Nanowire Hybrid Sponges for Highly Efficient Electromagnetic Interference Shielding. *Small* **2018**, *14*, 1800534.


https://doi.org/10.1021/acsami.1c16234
*ACS Appl. Mater. Interfaces* XXXX, XXX, XXX−XXX